Original Paper

MEASUREMENT AND CONTROL

Measurement and Control
2020, Vol. 53(5-6) 908–921

DOI: 10.1177/0020294020909126
journals.sagepub.com/home/mac
SAGE

Disturbance observer–based super-twisting sliding mode control for formation tracking of multi-agent mobile robots

Guigang Zhang[1], Yun Wang[1], Jian Wang[1], Jiarong Chen[2] and Dianwei Qian[2]

Abstract

This paper presents a super-twisting sliding mode control method for the formation maneuvers of multiple robots. In the real world of applications, the robots suffer from many uncertainties and disturbances that trouble the super-twisting sliding mode formation maneuvers very much. Especially, this issue has the adverse effects on the formation performance when the uncertainties and disturbances have an unknown bound. This paper focuses on this issue and utilizes the technique of disturbance observer to meet this challenge. In terms of the leader–follower framework, this paper investigates the integration of the super-twisting sliding mode control method and the disturbance observer technique. This kind of formation design has the guaranteed closed-loop stability in the sense of Lyapunov. Some simulations are implemented through a multi-robot platform. The results demonstrate that the superiority of the formation design regardless of uncertainties and disturbances.

Keywords

Mobile robots, formation control, super-twisting sliding mode control, uncertainties, disturbance observer

Date received: 6 October 2019; accepted: 31 January 2020

Introduction

Recently, multi-robot systems have paid great attention.[1] Compared with a complex robot, multi-robot systems are of merit. Not only such systems simplify individual robots, but also they are a platform to display collective behaviors.[2,3] Multi-robot systems have broad applications, including but not limited to search and rescue, military reconnaissance, and collaborative projects.[4,5]

In many cases, the achievement of a given task needs to form up multiple robots according to some patterns. In order to coordinate and supervise the robots, the formation problem raises up.[6] This problem is rooted from some biological systems. In weird nature, schools of fishes in swimming always form up some patterns in order to protect themselves as well as team of ants in moving.[7,8] As far as these biological systems are concerned, their formation patterns demonstrate strict hierarchy and high robustness because of the inherent existence of a certain formation mechanism.

Similarly, a multi-robot system also desires such a mechanism to coordinate the robots. It is reported that some typical mechanisms have been developed for multiple robots, that is, the virtual structure technique, the behavior-based algorithm, the artificial potential field approach, and the leader–follower framework.[9] Although the leader–follower framework among these typical mechanisms is criticized for its drawback of "single point of failure,"[10] this framework is well structured and even friendly from the aspect of control design. Especially, the leader–follower framework has visibly blossomed for the small- and medium-scale formation problem. Consequently, this paper does not focus on how to design a novel formation mechanism, but it works at the formation control design. Consequently, the leader–follower framework is directly adopted.

Considering the individual robots of a multi-robot system, they suffer from uncertainties and disturbances

[1]Institute of Automation, Chinese Academy of Sciences, Beijing, China
[2]School of Control and Computer Engineering, North China Electric Power University, Beijing, China

Corresponding author:
Guigang Zhang, Institute of Automation, Chinese Academy of Sciences, 95 Zhongguancun East Road, Beijing 100190, China.
Email: guigang.zhang@ia.ac.cn

from the viewpoint of reality. Without doubt, the formation dynamics of this multi-robot system become uncertain.[11,12] Affected by the adverse factors, the formation control problem of the multiple robots becomes interesting and challenging. Some control strategies have been reported, that is, iterative learning–based control methods,[13,14] model predictive formation control,[15] type-2 fuzzy formation control,[16,17] and so on.

The sliding mode control is a synthetic tool. It is alternative for the formation problem of uncertain multi-robot systems. Hitherto, some sliding mode–based control methods have been presented in the formation field of multiple robots, that is, the first-order sliding mode control,[18,19] the integral sliding mode control,[8] the derivative and integral terminal sliding mode control,[4] and the terminal sliding mode control.[20] With regard to the sliding mode control, its invariance is the most attractive property. This property can guarantee that a sliding mode control system is completely robust despite the matched uncertainties and disturbances.[21]

Actually, the sliding mode control is not perfect, and it is confronted with the dilemma of chattering. As a result, many ideas have been devoted to the decrease and elimination of chattering. Among these ideas, the super-twisting–based sliding mode control technique is advocated. Partly, it only needs the information of a sliding mode variable, and it gets rid of the dependence on the time derivative of this sliding mode variable.[22]

On the assumption that the bound of uncertainties and disturbances is known, this technique is able to effectively force the sliding mode variable and its time derivative to the origin in finite time.[23,24] Unfortunately, this assumption is not mild in terms of uncertain multi-robot systems. In reality, one has to overestimate this bound from the aspect of the closed-loop formation stability.[25,26] However, the overestimate definitely enlarges the gain of the super-twisting sliding mode control technique. A potential solution is to design a module that can estimate these uncertainties and disturbances.

Motivated by this solution, the disturbance observer technique[27] is taken into consideration. Inherently, the technique is a kind of compensation mechanisms because it can estimate the uncertainties and disturbances via some measurable information. The technique can contribute to the ability of disturbance attenuation for a control system. Concerning the super-twisting sliding mode formation maneuvers, it is possible to avoid the overestimate problem of the gain by the disturbance observer technique. So far, it is reported that the disturbance observer technique has been successfully applied to mechatronics systems,[28–31] chemical and process systems,[32] biological systems,[33] aerospace systems,[34] and so on. This paper adopts the technique for the super-twisting sliding mode formation maneuvers of uncertain multi-robot systems. The purpose is to refine the formation performance when the bound of the uncertainties and disturbances is unknown.

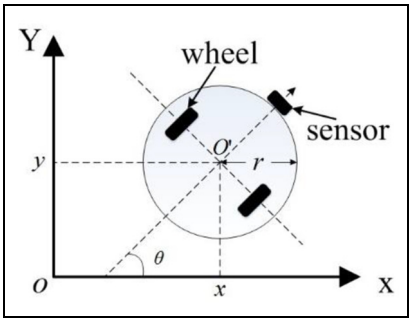

Figure 1. Sketches of the unicycle-like robot.

The remainder of this paper is organized as follows. Section "Formation model" models both a mobile robot and a leader–follower pair. Section "Formation design" addresses the super-twisting sliding mode control, adopts the disturbance observer technique to estimate the uncertainties and disturbances, and analyzes the closed-loop formation stability in the sense of Lyapunov. Section "Simulation results" implements the presented control method on a multi-robot system platform, and also illustrates some numerical results and comparisons. Finally, section "Conclusion" draws the conclusion.

Formation model

A mobile robot

The unicycle-like robot in Figure 1 moves in the horizontal plane. It is round and the diameter is $2r$. Its two parallel wheels have a same axis, independently controlled by two direct current motors. The robot can simultaneously rotate and translate, which is described by

$$\mathbf{q} = [x \quad y \quad \theta]^T \tag{1}$$

In equation (1), (x and y) located at the center of the robot represents its translational coordinates and θ indicates its rotational coordinate. To know the position, a positioning sensor at the front castor of this robot is set up. The axis of the sensor is orthogonal to the axis of the two wheels.

On the assumption of pure rolling and no slipping, the ideal kinematic model of this robot[4,8] has the form of

$$\dot{\mathbf{q}} = \begin{bmatrix} \dot{x} \\ \dot{y} \\ \dot{\theta} \end{bmatrix} = \begin{bmatrix} \cos\theta & 0 \\ \sin\theta & 0 \\ 0 & 1 \end{bmatrix} \cdot \begin{bmatrix} v \\ \omega \end{bmatrix} \tag{2}$$

$$\text{s.t.} \quad \dot{x}\sin\theta - \dot{y}\cos\theta = 0 \tag{3}$$

where v is the robot's linear velocity in the x–y coordinates and ω represents the angular velocity. The directions of the two vectors are that v is positive when the robot moves in the positive direction of the x-axis and that ω is positive when the robot rotates counterclockwise.

Concerning the constraint (3), the time derivative of equation (2), namely, the ideal dynamic model, can be written as

$$\begin{bmatrix} \ddot{x} \\ \ddot{y} \\ \ddot{\theta} \end{bmatrix} = \begin{bmatrix} -\dot{y}\dot{\theta} \\ \dot{x}\dot{\theta} \\ 0 \end{bmatrix} + \begin{bmatrix} \cos\theta & 0 \\ \sin\theta & 0 \\ 0 & 1 \end{bmatrix} \cdot \mathbf{u} \tag{4}$$

In equation (4), $\mathbf{u} = [\dot{v} \quad \dot{\omega}]^T$, in which the derivatives of v and ω represent the acceleration and the angular acceleration of the robot, respectively.

Since the robot in reality suffers from a variety of uncertainties and disturbances—for example, friction, slip, and slide shift—the real dynamic model[8] can be derived from equation (4)

$$\begin{bmatrix} \ddot{x} \\ \ddot{y} \\ \ddot{\theta} \end{bmatrix} = \begin{bmatrix} -\dot{y}\dot{\theta} \\ \dot{x}\dot{\theta} \\ 0 \end{bmatrix} + \begin{bmatrix} \cos\theta & 0 \\ \sin\theta & 0 \\ 0 & 1 \end{bmatrix} \cdot (\mathbf{u} + \Delta \cdot \mathbf{u}) + \boldsymbol{\pi}(\mathbf{q}, \dot{\mathbf{q}}) \tag{5}$$

In equation (5), the term $\boldsymbol{\pi}(\mathbf{q}, \dot{\mathbf{q}})$ represents the lumped uncertainties and disturbances, which is defined by

$$\boldsymbol{\pi}(\mathbf{q}, \dot{\mathbf{q}}) = [\pi_x \quad \pi_y \quad \pi_\theta]^T$$

where π_x, π_y, and π_θ are the functions of the vectors $\mathbf{q}$ and $\dot{\mathbf{q}}$. Δ indicates the physical parameter changes of this robot, which is described by

$$\Delta = \begin{bmatrix} \varepsilon & 0 \\ 0 & \varepsilon' \end{bmatrix}$$

where ε and ε' are the changes of the mass and the inertia of the robot, respectively.

A leader–follower pair

Consider a multi-robot system containing N robots. Each robot is the same as the robot in Figure 1. Without loss of generality, the robot i is selected as the leader, and it makes up $N-1$ leader–follower pairs with the left robots. Figure 2 illustrates such a leader–follower pair made of the leader i and the follower k.[8]

In Figure 2, the subscript i is adopted to label the individual variables of the leader, the subscript k is employed to describe the individual variables of the follower, and the subscript ik is used for the relative variables of this pair. Here, the relative distance l_{ik} means the distance between the leader's center and the follower's front castor, which is formulated by

$$l_{ik} = \sqrt{(x_i - \bar{x}_k)^2 + (y_i - \bar{y}_k)^2} \tag{6}$$

where

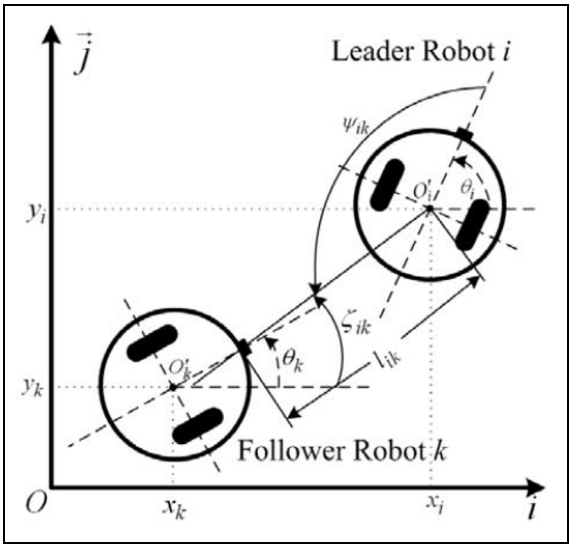

Figure 2. Sketches of a leader–follower pair.

$$\bar{x}_k = x_k + r\cos\theta_k$$
$$\bar{y}_k = y_k + r\sin\theta_k$$

The relative bearing angle ψ_{ik} of the leader–follower pair is determined by

$$\psi_{ik} = \pi + \zeta_{ik} - \theta_i \tag{7}$$

where

$$\zeta_{ik} = \arctan\frac{y_i - y_k - r\sin\theta_k}{x_i - x_k - r\cos\theta_k}$$

The purpose of the paper is to investigate the super-twisting sliding mode formation maneuvers of this multi-robot system via extreme learning machine (ELM). Motivated by the purpose, the formation objective of the leader–follower scheme is that each leader–follower pair of the multi-robot system has to keep the desired relative distance and the desired relative bearing angle in spite of uncertainties and disturbances. In order to focus on the objective, we consider some ideal conditions as follows: (1) there are neither collisions nor communication delays; and (2) the follower is well-known, that is, it knows its position and velocity, meanwhile, it can obtain the position and the velocity of the leader as well.

Formation dynamics by the first-order and second-order differential equations

Let

$$\mathbb{T}_{ik} = [l_{ik} \ \psi_{ik}]^T \tag{8}$$

In equation (8), the second derivatives of l_{ik} and ψ_{ik} with respect to time can be written by

$$\ddot{\mathbb{T}}_{ik} = \mathbb{G}_{ik}\mathbf{u}_k + \mathbb{D}_{ik} \tag{9}$$

where

$$\mathbb{G}_{ik} = \begin{bmatrix} \cos\varphi_{ik} & r\sin\varphi_{ik} \\ -\frac{\sin\varphi_{ik}}{l_{ik}} & \frac{r\cos\varphi_{ik}}{l_{ik}} \end{bmatrix}$$
$$\mathbb{L}_{ik} = \begin{bmatrix} -\cos\psi_{ik} & 0 \\ \frac{\sin\psi_{ik}}{l_{ik}} & -1 \end{bmatrix}$$
$$\mathbb{D}_{ik} = [\, D_{ik,1} \quad D_{ik,2}\,]^T = \mathbb{G}_{ik}\Delta_k\mathbf{u}_k + \mathbb{L}_{ik}(\mathbf{I}_2 + \Delta_i)\mathbf{u}_i + \mathbb{F}_{ik} + \mathbb{P}_{ik}$$
$$\mathbb{F}_{ik} = \begin{bmatrix} F_1 \\ F_2 \end{bmatrix}$$
$$\mathbb{P}_{ik} = \begin{bmatrix} P_1 \\ P_2 \end{bmatrix} \tag{10}$$

In equation (10), $\mathbf{I}_2 \in \Re^{2\times 2}$ is an identity matrix; $\varphi_{ik} = \psi_{ik} + \theta_{ik}$; and F_1, F_2, P_1, and P_2 have the form of

$$F_1 = \left(\dot{\psi}_{ik}\right)^2 l_{ik} + 2\dot{\psi}_{ik}\dot{\theta}_i l_{ik} + \left(\dot{\theta}_i\right)^2 l_{ik} - r\cos\varphi_{ik}\left(\dot{\theta}_k\right)^2 - \left(\dot{y}_k\dot{\theta}_k - \dot{y}_i\dot{\theta}_i\right)\cos\left(\psi_{ik} + \dot{\theta}_i\right) - \left(\dot{x}_i\dot{\theta}_i - \dot{x}_k\dot{\theta}_k\right)\sin(\psi_{ik} + \theta_i)$$
$$F_2 = \frac{-\left(\dot{y}_k\dot{\varphi}_{ik} - \dot{\psi}_{ik}\dot{y}_i\right)\sin(\psi_{ik} + \theta_i) - r\dot{\theta}_k\dot{\varphi}_{ik}\sin\varphi_{ik}}{l_{ik}}$$
$$\frac{-\left(\dot{x}_k\dot{\varphi}_{ik} - \dot{\psi}_{ik}\dot{x}_i\right)\cos(\psi_{ik} + \theta_i) + i_{ik}\left((\dot{y}_i - \dot{y}_k)\cos(\psi_{ik} + \theta_i) - (\dot{x}_i - \dot{x}_k)\sin(\psi_{ik} + \theta_i) - r\dot{\theta}_k\dot{\varphi}_{ik}\cos\varphi_{ik}\right)}{l_{ik}}$$
$$P_1 = -(\pi_{ix} - \pi_{kx})\cos(\psi_{ik} + \theta_i) - \left(\pi_{iy} - \pi_{ky}\right)\sin(\psi_{ik} + \theta_i) + r\pi_{k\theta}\sin\varphi_{ik}$$
$$P_2 = \frac{(\pi_{ix} - \pi_{kx})\sin(\psi_{ik} + \theta_i) - \left(\pi_{iy} - \pi_{ky}\right)\cos(\psi_{ik} + \theta_i) + r\pi_{k\theta}\sin\varphi_{ik} - l_{ik}\pi_{i\theta}}{l_{ik}}$$

Assumption 1. The vector $\mathbb{D}_{ik} \in \Re^{2\times 1}$ in equation (9) contains two parts, which is depicted by

$$\mathbb{D}_{ik} = \mathbb{D}_{ik0} + \mathbb{D}_{ik1} \tag{11}$$

Here, their ∞-norm satisfy

$$\|\mathbb{D}_{ik0}\|_\infty \leqslant \bar{\delta}_1 \text{ and } \left\|\dot{\mathbb{D}}_{ik1}\right\|_\infty \leqslant \bar{\delta}_2 \tag{12}$$

where $\mathbb{D}_{ik0}$ is the time-invariable part, and $\mathbb{D}_{ik1}$ is the time-variable part; both the parts are bounded, but $\bar{\delta}_1$ and δ_2 are unknown.

Define a vector $\mathbf{x}_{ik} = [x_1\, x_2\, x_3\, x_4]^{\mathrm{T}}$. Let $x_1 = l_{ik}$, $x_2 = \dot{l}_{ik}$, $x_3 = \psi_{ik}$, and $x_4 = \dot{\psi}_{ik}$. According to the formation objective, the relative distance l_{ik} and the relative bearing angle ψ_{ik} are determined as the formation control output. Then, the formation dynamics of this leader–follower pair in light of the leader–follower scheme can have the form of

$$\begin{aligned} \dot{\mathbf{x}}_{ik} &= \mathbf{f}(\mathbf{x}_{ik}, \mathbf{d}_{ik}, \Delta_k) + \mathbf{g}(\mathbf{x}_{ik})\mathbf{u}_k \\ \mathbf{y}_{ik} &= \mathbf{h}(\mathbf{x}_{ik}) \end{aligned} \tag{13}$$

where $\mathbf{x}_{ik}$ is the system state vector, and $\mathbf{y}_{ik}$ is the system output vector. Furthermore

$$\begin{aligned} \mathbf{f}(\mathbf{x}_{ik}, \mathbf{d}_{ik}, \Delta_k) &= \mathbf{A}_{ik}\mathbf{x}_{ik} + \mathbf{B}_{ik,2}\mathbf{d}_{ik} \\ \mathbf{g}(\mathbf{x}_{ik}) &= \mathbf{B}_{ik,1} \end{aligned} \tag{14}$$

$\mathbf{A}_{ik}$, $\mathbf{B}_{ik,1}$, $\mathbf{B}_{ik,2}$, and $\mathbf{h}(\mathbf{x}_{ik})$ are depicted by

$$\mathbf{A}_{ik} = \begin{bmatrix} 0 & 1 & 0 & 0 \\ 0 & 0 & 0 & 0 \\ 0 & 0 & 0 & 1 \\ 0 & 0 & 0 & 0 \end{bmatrix}, \quad \mathbf{B}_{ik,2} = \begin{bmatrix} 0 & 0 \\ 1 & 0 \\ 0 & 0 \\ 0 & 1 \end{bmatrix},$$
$$\mathbf{B}_{ik,1} = \begin{bmatrix} 0 & 0 \\ \cos\varphi_{ik} & r\sin\varphi_{ik} \\ 0 & 0 \\ \frac{-\sin\varphi_{ik}}{l_{ik}} & \frac{r\cos\varphi_{ik}}{l_{ik}} \end{bmatrix}, \mathbf{h}(\mathbf{x}_{ik}) = \begin{bmatrix} x_1 \\ x_3 \end{bmatrix}$$

$\mathbf{d}_{ik}$ has the form of

$$\mathbf{d}_{ik} = \mathbf{B}_{ik,1}\Delta_k\mathbf{u}_k + \mathbf{L}_{ik}(\mathbf{I}_2 + \Delta_i)\mathbf{u}_i + \mathbf{F}_{ik} + \mathbf{P}_{ik} \tag{15}$$

In equation (15)

$$\mathbf{L}_{ik} = \begin{bmatrix} 0 & 0 \\ -\cos\psi_{ik} & 0 \\ 0 & 0 \\ \frac{\sin\psi_{ik}}{l_{ik}} & -1 \end{bmatrix}, \quad \mathbf{F}_{ik} = \begin{bmatrix} 0 \\ F_1 \\ 0 \\ F_2 \end{bmatrix}, \quad \mathbf{P}_{ik} = \begin{bmatrix} 0 \\ P_1 \\ 0 \\ P_2 \end{bmatrix}$$

Both equations (9) and (13) describe the formation dynamics, where equation (9) is in the form of the second-order differential equations, and equation (13) has the expressions of the first-order differential equations. Inherently, they are equivalent to each other, and both of them can help the following control design.

Formation design

Sliding surfaces and input–output dynamics

The super-twisting law is a powerful and effective technique that can realize the second-order sliding mode control design. The technique can effectively deal with the controlled plant with a relative degree equal to one with respect to the control input. With regard to the matched uncertainties and disturbances, it can make the sliding mode variable and its time derivative convergent to the origin in finite time. Consequently, we consider this technique as a solution for formation maneuvers of the leader–follower pair in Figure 2. In order to implement the control design, the sliding surfaces—that is, the sliding mode vector—have to be predefined

$$\mathbf{s}_{ik} = \begin{bmatrix} s_{ik,1} \\ s_{ik,2} \end{bmatrix} = \mathbf{C}_1\mathbf{e}_{ik} + \mathbf{C}_2\dot{\mathbf{e}}_{ik} \tag{16}$$

where $\mathbf{e}_{ik} = [\, l_{ik} \quad \psi_{ik} \,]^T - [\, l_{ik}^d \quad \psi_{ik}^d \,]^T$, with l_{ik}^d and ψ_{ik}^d being the desired relative distance and the desired relative bearing angle of the leader–follower pair, respectively. $\mathbf{C}_1$ and $\mathbf{C}_2$ are the 2×2 constant diagonal matrices, which are given by

$$\mathbf{C}_1 = c_1\mathbf{I}_2 \text{ and } \mathbf{C}_2 = c_2\mathbf{I}_2 \tag{17}$$

where both c_1 and c_2 are the positive and the predefined constants.

Differentiate $\mathbf{s}_{ik}$ in equation (16) with the respect to time and substitute the formation dynamics equation (9) into the derivative of $\mathbf{s}_{ik}$. Then, the input–output dynamics are determined by

$$\dot{\mathbf{s}}_{ik} = \mathbf{C}_1\dot{\mathbf{e}}_{ik} + \mathbf{C}_2\ddot{\mathbf{e}}_{ik} \tag{18}$$

Substituting equation (9) into equation (18) yields

$$\dot{\mathbf{s}}_{ik} = \mathbf{C}_1\dot{\mathbf{e}}_{ik\,ik} + \mathbf{C}_2\mathbb{D}_{ik} + \mathbf{C}_2\mathbb{G}_{ik}\mathbf{u}_k \tag{19}$$

In order to achieve the super-twisting sliding mode control design, the first step is to calculate the relative degree of the dynamics equation (14) with respect to the control input. From equations (16) and (19), we obtain

$$\frac{\partial \mathbf{s}_{ik}}{\partial \mathbf{u}_k} = 0 \text{ and } \frac{\partial \dot{\mathbf{s}}_{ik}}{\partial \mathbf{u}_k} = \mathbf{C}_2\mathbb{G}_{ik} \neq 0 \tag{20}$$

From equation (20), it is apparent that the relative degree of $\mathbf{s}_{ik}$ with respect to $\mathbf{u}_k$ is equal to 1. In other words, the super-twisting sliding mode control design is available for formation maneuvers under the leader–follower scheme.

Super-twisting sliding mode control design

Let $\dot{\mathbf{s}}_{ik} = \varpi_k$ in equation (17). Then, the super-twisting sliding mode control for the nominal formation of the leader–follower pair can be designed as

$$\mathbf{u}_k = (\mathbf{C}_2\mathbb{G}_{ik})^{-1}(\varpi_k - \mathbf{C}_1\dot{\mathbf{e}}_{ik}) \tag{21}$$

where

$$\begin{aligned} &\varpi_k = \varpi_{k1} + \varpi_{k2} \\ &\varpi_{k1} = -\alpha_k\sqrt{\|\mathbf{s}_{ik}\|_2}\,\mathrm{sgn}(\mathbf{s}_{ik}) \text{ and } \varpi_{k2} = -\chi_k\mathrm{sgn}(\mathbf{s}_{ik}) \end{aligned} \tag{22}$$

In equation (21), α_k and χ_k are positive, which need to be predefined. The signum function $\mathrm{sgn}(\mathbf{s}_{ik})$ in equation (22) is defined by $\mathrm{sgn}(\mathbf{s}_{ik}) = [\, \mathrm{sgn}(s_{ik,1}) \quad \mathrm{sgn}(s_{ik,2}) \,]^T$. Select a Lyapunov function equation (23)

$$V_0 = \|\mathbf{s}_{ik}\|_2 \tag{23}$$

Note $\|\mathbf{s}_{ik}\|_1 = \mathbf{s}_{ik}^T\mathrm{sgn}(\mathbf{s}_{ik})$ and $\int_0^t \mathrm{sgn}(\mathbf{s}_{ik})\mathrm{d}t = \mathrm{sgn}(\mathbf{s}_{ik})\int_0^t \mathrm{d}t$. On Assumption 1, substituting equations (21) and (22) into the time derivative of equation (23) yields

$$\begin{aligned} \dot{V}_0 &= \frac{\mathbf{s}_{ik}^T\dot{\mathbf{s}}_{ik}}{\|\mathbf{s}_{ik}\|_2} = \frac{\mathbf{s}_{ik}^T}{\|\mathbf{s}_{ik}\|_2}(\mathbf{C}_1\dot{\mathbf{e}}_{ik} + \mathbf{C}_2\mathbb{D}_{ik} + \mathbf{C}_2\mathbb{G}_{ik}\mathbf{u}_k) \\ &= \frac{\mathbf{s}_{ik}^T}{\|\mathbf{s}_{ik}\|_2}(\varpi_k + \mathbf{C}_2\mathbb{D}_{ik}) \\ &= \frac{\mathbf{s}_{ik}^T}{\|\mathbf{s}_{ik}\|_2}\left(-\alpha_k\sqrt{\|\mathbf{s}_{ik}\|_2}\mathrm{sgn}(\mathbf{s}_{ik}) - \chi_k\mathrm{sgn}(\mathbf{s}_{ik})\int_0^t \mathrm{d}t + \mathbf{C}_2\mathbb{D}_{ik}\right) \\ &= -\frac{\alpha_k\sqrt{\|\mathbf{s}_{ik}\|_2}}{\|\mathbf{s}_{ik}\|_2}\|\mathbf{s}_{ik}\|_1 - \frac{\chi_k}{\|\mathbf{s}_{ik}\|_2}\|\mathbf{s}_{ik}\|_1 \\ &\quad \int_0^t \mathrm{d}t + c_2\frac{\mathbf{s}_{ik}^T}{\|\mathbf{s}_{ik}\|_2}(\mathbb{D}_{ik0} + \mathbb{D}_{ik1}) \\ &= -\frac{\alpha_k\sqrt{\|\mathbf{s}_{ik}\|_2}}{\|\mathbf{s}_{ik}\|_2}\|\mathbf{s}_{ik}\|_1 + c_2\frac{\mathbf{s}_{ik}^T}{\|\mathbf{s}_{ik}\|_2}\mathbb{D}_{ik0} - \frac{\chi_k}{\|\mathbf{s}_{ik}\|_2}\|\mathbf{s}_{ik}\|_1 \\ &\quad \int_0^t \mathrm{d}t + c_2\frac{\mathbf{s}_{ik}^T}{\|\mathbf{s}_{ik}\|_2}\int_0^t \dot{\mathbb{D}}_{ik1}\mathrm{d}t \\ &\leqslant \frac{\sqrt{\|\mathbf{s}_{ik}\|_2}}{\|\mathbf{s}_{ik}\|_2}\|\mathbf{s}_{ik}\|_1(-\alpha_k + c_2\delta_1) + \frac{\|\mathbf{s}_{ik}\|_1}{\|\mathbf{s}_{ik}\|_2}\int_0^t (-\chi_k + c_2\delta_2)\mathrm{d}t \end{aligned} \tag{24}$$

where $\delta_1 = \bar{\delta}/\sqrt{||\mathbf{s}_{ik}||_{21}}$.

Concerning equation (24), one can have $\dot{V}_0 < 0$ by picking up α_k and χ_k if δ_1 and δ_2 are known. Unfortunately, these constants are hardly known in advance, that is, equation (21) theoretically holds true but it is not available in reality. In order to make equation (21) hold true, one possible approach is to overestimate α_k and χ_k so that $\dot{V}_0 < 0$ can be guaranteed and the closed-loop formation system can have the stability in the sense of Lyapunov. However, the approach inevitably enlarges the gain of the super-twisting sliding mode control technique, which can definitely have the adverse effects on the formation performance. For this issue, this paper touches the disturbance observer technique and fuses it with the super-twisting sliding mode control, where the disturbance observer can estimate the uncertainties and disturbances online. Their integration can guarantee the formation stability while the super-twisting sliding mode control technique can have a suitable gain.

Design of disturbance observer

From equation (12), it is apparent that $\mathbb{D}_{ik}$ contains two parts, that is, the time-invariant and time-variant parts. Concerning the time-invariant component $\mathbb{D}_{ik0}$, we have $\dot{\mathbb{D}}_{ik0} \equiv 0$. For the time-variant component $\mathbb{D}_{ik1}$, we have the following assumption.

Assumption 2. Compared with the dynamic characteristics of the disturbance observer, the change rate of the time-variable component $\mathbb{D}_{ik1}$ is slow, that is, $\dot{\mathbb{D}}_{ik1} \simeq 0$ exists in the formation dynamics from the viewpoint of the observer dynamics.

The fulfillment of the disturbance observer needs to define the observer dynamics so that we define the disturbance observer as

$$\begin{aligned}\dot{\mathbf{p}}_{ik} &= -\mathbf{L}_{ik}\mathbf{B}_{ik,2}\mathbf{p}_{ik} - \mathbf{L}_{ik}(\mathbf{B}_{ik,2}\mathbf{L}_{ik}\mathbf{x}_{ik} + \mathbf{A}_{ik}\mathbf{x}_{ik} + \mathbf{B}_{ik,1}\mathbf{u}_k)\\ \hat{\mathbb{D}}_{ik} &= \mathbf{p}_{ik} + \mathbf{L}_{ik}\mathbf{x}_{ik}\end{aligned} \tag{25}$$

where $\mathbf{p}_{ik} \in \Re^{2\times 1}$ is the state vector of the disturbance observer; $\hat{\mathbb{D}}_{ik} \in \Re^{2\times 1}$ is the estimate of the real disturbance vector $\mathbb{D}_{ik}$; and $\mathbf{L}_{ik} \in \Re^{2\times 4}$ is the gain matrix of the disturbance observer, which needs to be predefined from the aspect of the observer stability.

Now, let us consider the observer stability. This disturbance observer is employed to estimate the disturbances and uncertainties so that the estimate errors are adopted to evaluate the observer stability. Define the estimate error vector as

$$\mathbf{e}_{\mathbb{D}ik} = [\, e_{\mathbf{D}ik,1} \quad e_{\mathbf{D}ik,2}\,]^T = \mathbb{D}_{ik} - \hat{\mathbb{D}}_{ik} \tag{26}$$

On Assumptions 1 and 2, the time derivative of $\mathbf{e}_{\mathbb{D}ik}$ in equation (26) yields

$$\begin{aligned}\dot{\mathbf{e}}_{\mathbb{D}ik} &= \dot{\mathbb{D}}_{ik} - \dot{\hat{\mathbb{D}}}_{ik}\\ &= \dot{\mathbb{D}}_{ik0} + \dot{\mathbb{D}}_{ik1} - \dot{\hat{\mathbb{D}}}_{ik}\\ &\simeq -\dot{\hat{\mathbb{D}}}_{ik} = -\dot{\mathbf{p}}_{ik} - \mathbf{L}_{ik}\dot{\mathbf{x}}_{ik}\\ &= \mathbf{L}_{ik}\mathbf{B}_{ik,2}\mathbf{p}_{ik} + \mathbf{L}_{ik}(\mathbf{B}_{ik,2}\mathbf{L}_{ik}\mathbf{x}_{ik} + \mathbf{A}_{ik}\mathbf{x}_{ik} + \mathbf{B}_{ik,1}\mathbf{u}_k)\\ &\quad - \mathbf{L}_{ik}(\mathbf{A}_{ik}\mathbf{x}_{ik} + \mathbf{B}_{ik,1}\mathbf{u}_k + \mathbf{B}_{ik,2}\mathbf{d}\mathbb{D}_{ik})\\ &= \mathbf{L}_{ik}\mathbf{B}_{ik,2}\left(\hat{\mathbb{D}}_{ik} - \mathbf{L}_{ik}\mathbf{x}_{ik}\right)\\ &\quad + \mathbf{L}_{ik}(\mathbf{B}_{ik,2}\mathbf{L}_{ik}\mathbf{x}_{ik} + \mathbf{A}_{ik}\mathbf{x}_{ik} + \mathbf{B}_{ik,1}\mathbf{u}_k)\\ &\quad - \mathbf{L}_{ik}(\mathbf{A}_{ik}\mathbf{x}_{ik} + \mathbf{B}_{ik,1}\mathbf{u}_k + \mathbf{B}_{ik,2}\mathbb{D}_{ik})\\ &= \mathbf{L}_{ik}\mathbf{B}_{ik,2}\left(\hat{\mathbb{D}}_{ik} - \mathbb{D}_{ik}\right) = -\mathbf{L}_{ik}\mathbf{B}_{ik,2}\mathbf{e}_{\mathbb{D}ik}\end{aligned} \tag{27}$$

The solution of $\dot{\mathbf{e}}_{\mathbb{D}ik} = -\mathbf{L}_{ik}\mathbf{B}_{ik,2}\mathbf{e}_{\mathbb{D}ik}$ has the form of

$$\mathbf{e}_{\mathbb{D}ik} = \exp(-\mathbf{H}_{ik}t)\mathbf{e}_{\mathbb{D}ik}(0) \tag{28}$$

In equation (28), $\mathbf{H}_{ik} = \mathbf{L}_{ik}\mathbf{B}_{ik,2}$. Select $\mathbf{L}_{ik}$ so that all the eigenvalues of $\mathbf{H}_{ik}$ are positive. This fact indicates that the estimate error $\mathbf{e}_{\mathbb{D}ik}$ may be exponentially convergent to $[\,0 \quad 0\,]^T$ as $t \to \infty$.

Super-twisting sliding mode control via disturbance observer

With regard to the disturbance observer, $\dot{\mathbf{e}}_{\mathbb{D}ik}$ is strictly equal to $-\mathbf{L}_{ik}\mathbf{B}_{ik,2}\mathbf{e}_{\mathbb{D}ik}$ in equation (27). They are just approximately equal. Thus, $\mathbf{e}_{\mathbb{D}ik}$ in equation (27) can be exponentially convergent to $[\,0 \quad 0\,]^T$ as $t \to \infty$ if $\mathbf{e}_{\mathbb{D}ik}(0)$ is finite. To deal with the issue, the following mild assumption is taken into consideration.

Assumption 3. The estimate error vector $\mathbf{e}_{\mathbb{D}ik}$ is bounded by $\|\mathbf{e}_{\mathbb{D}ik}\|_\infty \leqslant e^*_{\mathbb{D}}$, in which $e^*_{\mathbb{D}} > 0$ is unknown.

In order to integrate the super-twisting sliding mode control method and the disturbance observer technique, we revise the sliding surfaces equation (16) and introduce the estimate vector $\hat{\mathbb{D}}_{ik}$ into the sliding surfaces so that the redefined sliding surfaces have the form of

$$\mathbf{s}_{ik} = \mathbf{C}_1\mathbf{e}_{ik} + \mathbf{C}_2\dot{\mathbf{e}}_{ik} + \hat{\mathbb{D}}_{ik} \tag{29}$$

In equation (29), differentiate $\mathbf{s}_{ik}$ with respect to time. Then, the input–output dynamics of the sliding surfaces can be obtained by

$$\dot{\mathbf{s}}_{ik} = \mathbf{C}_1\dot{\mathbf{e}}_{ik} + \mathbf{C}_2\ddot{\mathbf{e}}_{ik} + \dot{\hat{\mathbb{D}}}_{ik} \tag{30}$$

Substituting the formation dynamics equation (9) into equation (30) yields

$$\dot{\mathbf{s}}_{ik} = \mathbf{C}_1\dot{\mathbf{e}}_{ik} + \mathbf{C}_2(\mathbb{G}_{ik}\mathbf{u}_k + \mathbb{D}_{ik}) + \dot{\hat{\mathbb{D}}}_{ik} \tag{31}$$

Select the super-twisting sliding mode control via the disturbance observer as

$$\begin{aligned}\mathbf{u}_k &= (\mathbf{C}_2\mathbb{G}_{ik})^{-1}\\ &\left(-\alpha_k\sqrt{\|\mathbf{s}_{ik}\|_2}\,\mathrm{sgn}(\mathbf{s}_{ik}) - \int_0^t \chi_k\,\mathrm{sgn}(\mathbf{s}_{ik})\mathrm{d}t - \mathbf{C}_2\dot{\hat{\mathbb{D}}}_{ik} - \mathbf{C}_1\dot{\mathbf{e}}_{ik}\right)\end{aligned} \tag{32}$$

where α_k and χ_k are positive, which are determined by the following Theorem 1.

Replacing $\mathbf{u}_k$ in equation (31) by equation (32) gives

$$\begin{aligned}\dot{\mathbf{s}}_{ik} &= -\alpha_k\sqrt{\|\mathbf{s}_{ik}\|_2}\,\mathrm{sgn}(\mathbf{s}_{ik})\\ &\quad - \int_0^t \chi_k\,\mathrm{sgn}(\mathbf{s}_{ik})\mathrm{d}t + \mathbf{C}_2\left(\mathbb{D}_{ik} - \hat{\mathbb{D}}_{ik}\right) + \dot{\hat{\mathbb{D}}}_{ik}\end{aligned} \tag{33}$$

Theorem 1. Concerning the leader–follower pair, its formation dynamics on Assumptions 1, 2, and 3 are determined by equations (9) and (13), its disturbance observer is designed by equation (25), its sliding surface vector is described by equation (29), and its super-twisting sliding mode control law via the disturbance observer is given by equation (32). Then, the closed-loop control system of this pair becomes asymptotically stable despite the uncertainties and disturbances if equation (34) holds true

$$\begin{aligned}&\alpha_k > \|\mathbf{C}_2 + \mathbf{H}_{ik}\|_\infty e^*_{\mathbb{D}}\\ &\chi_k > 0\end{aligned} \tag{34}$$

Proof. Similarly, we also pick up the Lyapunov function as equation (23), differentiate it with respect to time, and replace the time derivative of $\mathbf{s}_{ik}$ by equation (33). Then, we can obtain

$$\begin{aligned}\dot{V} &= \frac{\mathbf{s}_{ik}^T\dot{\mathbf{s}}_{ik}}{\|\mathbf{s}_{ik}\|_2} = \frac{\mathbf{s}_{ik}^T}{\|\mathbf{s}_{ik}\|_2}\\ &\left(-\alpha_k\sqrt{\|\mathbf{s}_{ik}\|_2}\,\mathrm{sgn}(\mathbf{s}_{ik}) - \int_0^t \chi_k\,\mathrm{sgn}(\mathbf{s}_{ik})\mathrm{d}t + \mathbf{C}_2\left(\mathbb{D}_{ik} - \hat{\mathbb{D}}_{ik}\right) + \dot{\hat{\mathbb{D}}}_{ik}\right)\end{aligned} \tag{35}$$

From equation (27), there exists

$$\dot{\hat{\mathbb{D}}}_{ik} = -\mathbf{H}_{ik}\left(\hat{\mathbb{D}}_{ik} - \mathbb{D}_{ik}\right) \tag{36}$$

Substituting equation (36) into equation (35) yields

$$\begin{aligned}\dot{V} &= \frac{\mathbf{s}_{ik}^T\dot{\mathbf{s}}_{ik}}{\|\mathbf{s}_{ik}\|_2} = \frac{\mathbf{s}_{ik}^T}{\|\mathbf{s}_{ik}\|_2} \\ &\left(-\alpha_k\sqrt{\|\mathbf{s}_{ik}\|_2}\mathrm{sgn}(\mathbf{s}_{ik}) - \int_0^t \chi_k\mathrm{sgn}(\mathbf{s}_{ik})\mathrm{d}t + (\mathbf{C}_2 + \mathbf{H}_{ik})\left(\mathbb{D}_{ik} - \hat{\mathbb{D}}_{ik}\right)\right) \\ &= -\frac{\alpha_k\sqrt{\|\mathbf{s}_{ik}\|_2}}{\|\mathbf{s}_{ik}\|_2}\mathbf{s}_{ik}^T\mathrm{sgn}(\mathbf{s}_{ik}) - \frac{\chi_k\int_0^t \mathrm{d}t}{\|\mathbf{s}_{ik}\|_2}\mathbf{s}_{ik}^T\mathrm{sgn}(\mathbf{s}_{ik}) \\ &+ \frac{\mathbf{s}_{ik}^T}{\|\mathbf{s}_{ik}\|_2}(\mathbf{C}_2 + \mathbf{H}_{ik})\left(\mathbb{D}_{ik} - \hat{\mathbb{D}}_{ik}\right)\end{aligned} \tag{37}$$

According to equation (26) and the concepts of vector norm, equation (37) can be written by

$$\begin{aligned}\dot{V} = &-\frac{\alpha_k\sqrt{\|\mathbf{s}_{ik}\|_2}}{\|\mathbf{s}_{ik}\|_2}\|\mathbf{s}_{ik}\|_1 \\ &-\frac{\chi_k\int_0^t \mathrm{d}t}{\|\mathbf{s}_{ik}\|_2}\|\mathbf{s}_{ik}\|_1 + \frac{\mathbf{s}_{ik}^T}{\|\mathbf{s}_{ik}\|_2}(\mathbf{C}_2 + \mathbf{H}_{ik})\mathbf{e}_{\mathbb{D}ik}\end{aligned} \tag{38}$$

Concerning Assumption 3, equation (38) has the form of

$$\begin{aligned}\dot{V} &\leqslant -\frac{\alpha_k\sqrt{\|\mathbf{s}_{ik}\|_2}}{\|\mathbf{s}_{ik}\|_2}\|\mathbf{s}_{ik}\|_1 - \frac{\chi_k\int_0^t \mathrm{d}t}{\|\mathbf{s}_{ik}\|_2}\|\mathbf{s}_{ik}\|_1 \\ &+ \frac{\mathbf{s}_{ik}^T}{\|\mathbf{s}_{ik}\|_2}\begin{bmatrix}\|(\mathbf{C}_2 + \mathbf{H}_{ik})\mathbf{e}_{\mathbb{D}ik}\|_\infty \\ \|(\mathbf{C}_2 + \mathbf{H}_{ik})\mathbf{e}_{\mathbb{D}ik}\|_\infty\end{bmatrix} \\ &= -\frac{\alpha_k\sqrt{\|\mathbf{s}_{ik}\|_2}}{\|\mathbf{s}_{ik}\|_2}\|\mathbf{s}_{ik}\|_1 - \frac{\chi_k\int_0^t \mathrm{d}t}{\|\mathbf{s}_{ik}\|_2}\|\mathbf{s}_{ik}\|_1 \\ &+ \frac{\|(\mathbf{C}_2 + \mathbf{H}_{ik})\mathbf{e}_{\mathbb{D}ik}\|_\infty}{\|\mathbf{s}_{ik}\|_2}\mathbf{s}_{ik}^T\begin{bmatrix}1 \\ 1\end{bmatrix} \\ &\leqslant -\alpha_k\sqrt{\|\mathbf{s}_{ik}\|_2}\frac{\|\mathbf{s}_{ik}\|_1}{\|\mathbf{s}_{ik}\|_2} - \chi_k\int_0^t \mathrm{d}t\frac{\|\mathbf{s}_{ik}\|_1}{\|\mathbf{s}_{ik}\|_2} \\ &+ \|(\mathbf{C}_2 + \mathbf{H}_{ik})\mathbf{e}_{\mathbb{D}ik}\|_\infty\frac{\|\mathbf{s}_{ik}\|_1}{\|\mathbf{s}_{ik}\|_2} \\ &\leqslant -\alpha_k\sqrt{\|\mathbf{s}_{ik}\|_2}\frac{\|\mathbf{s}_{ik}\|_1}{\|\mathbf{s}_{ik}\|_2} - \chi_k\int_0^t \mathrm{d}t\frac{\|\mathbf{s}_{ik}\|_1}{\|\mathbf{s}_{ik}\|_2} \\ &+ \|(\mathbf{C}_2 + \mathbf{H}_{ik})\|_\infty\|\mathbf{e}_{\mathbb{D}ik}\|_\infty\frac{\|\mathbf{s}_{ik}\|_1}{\|\mathbf{s}_{ik}\|_2} \\ &= \left[-\alpha_k\sqrt{\|\mathbf{s}_{ik}\|_2} - \chi_k\int_0^t \mathrm{d}t + \|(\mathbf{C}_2 + \mathbf{H}_{ik})\|_\infty e_{\mathbb{D}}^*\right]\frac{\|\mathbf{s}_{ik}\|_1}{\|\mathbf{s}_{ik}\|_2}\end{aligned} \tag{39}$$

In equation (39), we will have $\dot{V} < 0$ if equation (34) holds true. This indicates that the leader–follower pair is of asymptotically stable in the sense of Lyapunov.

Compared with equations (24) and (39), both of $\dot{V} < 0$ are dependent on α_k and χ_k. But the two control approaches make some difference to each other. In equation (24), α_k and χ_k have to be overestimated from the aspect of the closed-loop stability, the gain of the super-twisting sliding mode control can be enlarged, and the formation performance may be deteriorated. On the contrary, α_k and χ_k are still unknown in equation (39), which also need to be estimated. However, we know that χ_k can be an arbitrary positive constant and that $\alpha_k > 0$ is related to $e_{\mathbb{D}}^*$. Although $e_{\mathbb{D}}^*$ is still kept unknown, it can be exponentially convergent if the estimate error vector $\mathbf{e}_{\mathbb{D}ik}$ is bounded.

Finally, the structure of the closed-loop formation system is displayed in Figure 3. From Figure 3, it is apparent that both the sliding surface vector and the observer employ the states of the formation dynamics to calculate the sliding surfaces and the disturbance estimation, and that they feed the super-twisting sliding mode controller located at the feedback channel to achieve the formation task.

Simulation results

Platform

This section will integrate the super-twisting sliding mode control method and the disturbance observer technique for an uncertain multi-robot system. In order to verify the presented method, we only consider the small-scale formation so that a multi-robot simulation platform with three mobile robots is taken into consideration. The Robot 1 acts as the leader, the Robot 2 and the Robot 3 act as the followers, and there are two leader–follower pairs in this platform. The two followers are coordinated by the leader. In the small-scale multi-robot system, some assumptions such as no collisions and no communication delay can easily hold true so that we can focus on the formation control design and investigate the feasibility of the disturbance observer–based super-twisting sliding mode control method.

The diameter of these robots is set to 0.10 m. This size is large enough for the robots to carry some sensors. The uncertainties in each robot are set by

$$\Delta_1 = \Delta_2 = \Delta_3 = \begin{bmatrix}\bar{\Delta} & 0 \\ 0 & \bar{\Delta}\end{bmatrix} \tag{40}$$

where $\bar{\Delta}$ is determined by $0.3\times\mathrm{rad} - 0.2$, and the rad means a random number in the closed interval [0 1]. In equation (5), $\bar{\Delta}$ is concerned to the changes of the robots' physical parameters. Here, we assume that they are the same.

Equation (9) contains $\pi_{ix} - \pi_{kx}$ and $\pi_{iy} - \pi_{ky}$ so that it is not representative to choose $\boldsymbol{\pi}_i = \boldsymbol{\pi}_k$. Concerning this multi-robot platform, we pick them up as

$$\pi_{1x} = \pi_{1y} = \pi_{1\theta} = 0.5\sin(2\pi t) \tag{41}$$

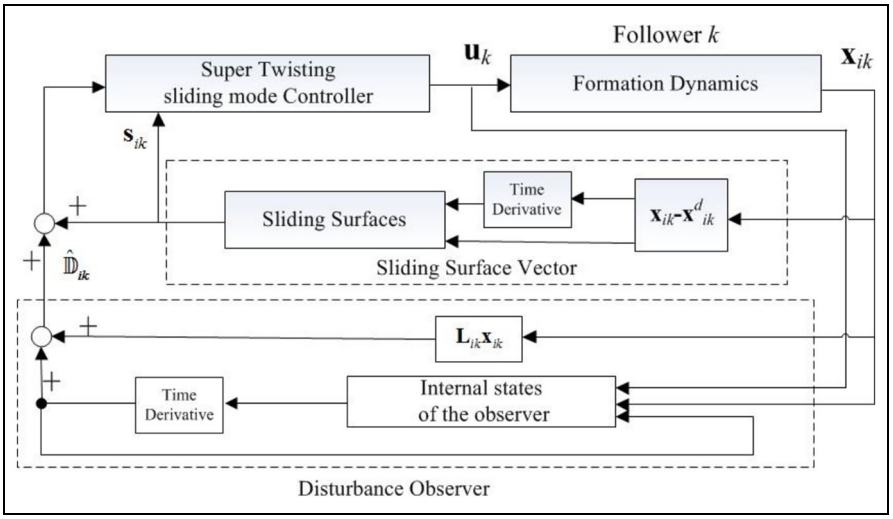

Figure 3. Structure of the disturbance observer–based super-twisting sliding mode control system.

$$\pi_{2x} = \pi_{2y} = \pi_{2\theta} = \pi_{3x} = \pi_{3y} = \pi_{3\theta} = 0.3\sin(2\pi t) \tag{42}$$

As far as the formation tasks of this multi-robot system are concerned, the leader takes charge of tracking a desired trajectory while the two followers keep the desired relative distance and the desired relative bearing angle with respect to the leader. Shown in equation (9), the designed control method is applied to the followers that fulfill the formation tasks. Meanwhile, the leader just tracks and maintains a desired trajectory regardless of the followers.

In general, the same parameters of the super-twisting sliding mode control and the disturbance observer are chosen for the two followers. Considering the super-twisting sliding mode control, the parameters are determined by $\alpha_2 = \alpha_3 = 18$, $\chi_2 = \chi_3 = 80$, $\mathbf{C}_1 = 1600\mathbf{I}_2$, and $\mathbf{C}_2 = 78\mathbf{I}_2$, respectively. Concerning the disturbance observer, its gain matrix is depicted by

$$\mathbf{L}_{12} = \mathbf{L}_{13} = \begin{bmatrix} 0 & 2 & 0 & 2 \\ 0 & 2 & 0 & 2 \end{bmatrix}$$

Simulations

Triangular formation moving along a straight line. In Figure 4, the multi-robot platform carries out the task of triangular formation when moving along a straight line trajectory, in which the red means the leader robot and the green and the blue delegate the two followers. The initial postures of the three robots are allocated at

$$\begin{aligned} \mathbf{q}_1 &= [0\,\text{m} \quad 0.5\,\text{m} \quad 0.5\pi\text{rad}]^T, \\ \mathbf{q}_2 &= [-0.4\,\text{m} \quad 0.8\,\text{m} \quad 0\text{rad}]^T, \text{ and} \\ \mathbf{q}_3 &= [-0.5\,\text{m} \quad 1.1\,\text{m} \quad 0.33\pi\text{rad}]^T \end{aligned} \tag{43}$$

According to the initial postures equation (43) and the formation task, the initial states of the formation dynamics equation (13) can be calculated as

$$\begin{aligned} \mathbf{x}_{12}(0) &= [0.46\,\text{m} \quad 0\,\text{m/s} \quad 1.22\pi\text{rad} \quad 0\text{rad/s}]^T \\ \text{and } \mathbf{x}_{13}(0) &= [0.77\,\text{m} \quad 0\,\text{m/s} \quad 1.30\pi\text{rad} \quad 0\text{rad/s}]^T \end{aligned} \tag{44}$$

In accordance with the formation task, the desired states can be determined by

$$\begin{aligned} \mathbf{x}^d_{12} &= [0.3\text{m} \quad 0\text{m/s} \quad 1.3\pi\text{rad} \quad 0\text{rad/s}]^T \\ \text{and } \mathbf{x}^d_{13} &= [0.6\text{m} \quad 0\text{m/s} \quad 1.7\pi\text{rad} \quad 0\text{rad/s}]^T \end{aligned} \tag{45}$$

Figure 5 demonstrates the state variables when the multi-robot system fulfills the formation task in Figure 4. For the purpose of comparisons, the other two classic control methods are also implemented on the same platform to accomplish the same formation task besides

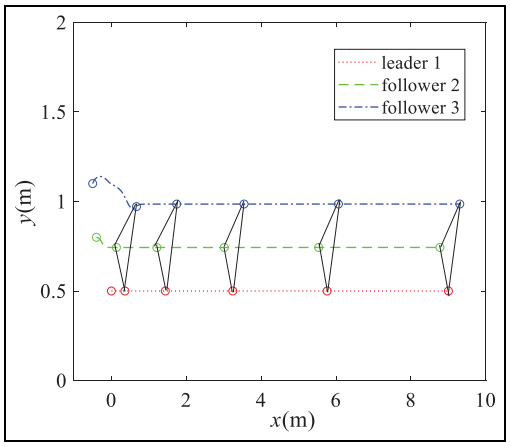

Figure 4. Triangular formation of the multi-robot system while moving along a straight line.

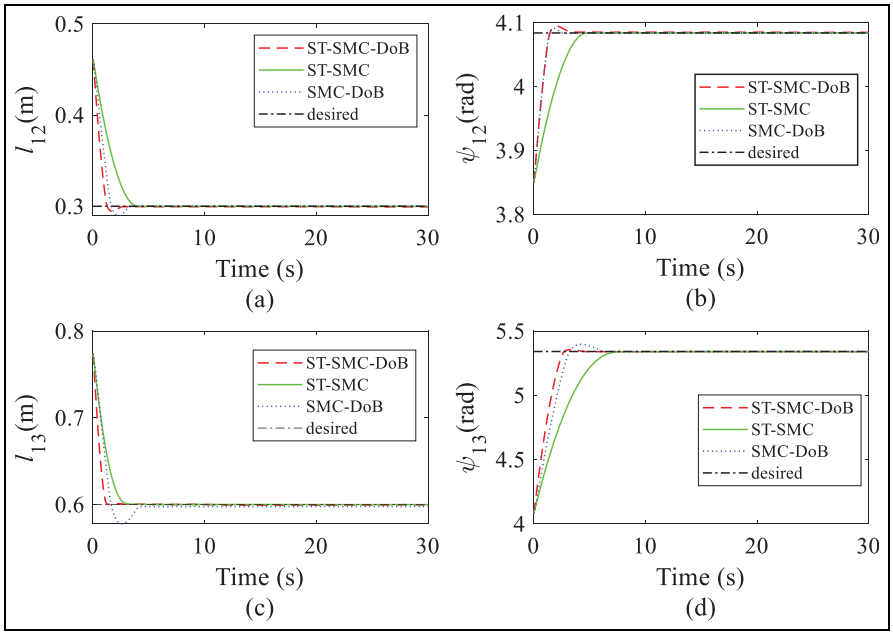

Figure 5. Comparisons of the state variables by different methods: (a) l_{12}, (b) ψ_{12}, (c) l_{13}, and (d) ψ_{13}.

the presented integration (short for ST-SMC-DoB in Figure 5). These control methods are listed as the sliding mode control with disturbance observer[18] (short for SMC-DoB in Figure 5) and the sole super-twisting sliding mode control without ELM (short for ST-SMC in Figure 5). From Figure 5, the presented method can improve the performance of the system state variables. Note that the sole super-twisting sliding mode control is with the same sliding surfaces formulated by equation (11). From this aspect, the disturbance observer technique can benefit the improvement of the control performance.

The control inputs of the three control methods applied to the follower 2 and the follower 3 are illustrated in Figures 6 and 7, respectively. In Figures 6 and 7, the presented method can decrease the chattering phenomenon effectively. In theory, the integrated method can compensate the disturbances and uncertainties entering the formation control system.

Figure 8 illustrates the sliding surfaces. The estimations of uncertainties and the estimation errors are illustrated in Figures 9 and 10. Proven in Theorem 1, the formation control system is asymptotically stable. From Figure 10, we know the errors are large at the outset, but they are dramatically decreased with respect to time.

Triangular formation moving along a circular trajectory. This platform in Figure 11 forms up a triangle when moving along a circular trajectory. Both the super-twisting sliding mode control parameters and the ELM parameters are kept unchanged. They are the same as the formation task in Figure 4. Concerning this task, the initial postures of the three robots are set by

$$\mathbf{q}_1 = [0.5\,\mathrm{m} \quad 0\,\mathrm{m} \quad 0.5\pi\mathrm{rad}]^T,$$
$$\mathbf{q}_2 = \left[0.8\,\mathrm{m} \quad -0.2\,\mathrm{m} \quad \frac{1}{3}\pi\mathrm{rad}\right]^T, \text{and}$$
$$\mathbf{q}_3 = [1.1\,\mathrm{m} \quad -0.3\,\mathrm{m} \quad \pi\mathrm{rad}]^T \tag{46}$$

According to this control task and the initial postures, the initial states of the formation dynamics can be calculated by

$$\mathbf{x}_{12}(0) = [0.36\,\mathrm{m} \quad 0\,\mathrm{m/s} \quad 1.36\pi\mathrm{rad} \quad 0\ \mathrm{rad/s}]^T \text{ and}$$
$$\mathbf{x}_{13}(0) = [0.63\,\mathrm{m} \quad 0\,\mathrm{m/s} \quad 1.34\pi\mathrm{rad} \quad 0\ \mathrm{rad/s}]^T \tag{47}$$

Similarly, the desired states can be obtained on account of the leader's trajectory

$$\mathbf{x}_{12}^d = [0.13\,\mathrm{m} \quad 0\,\mathrm{m/s} \quad 1.8\pi\mathrm{rad} \quad 0\ \mathrm{rad/s}]^T \text{ and}$$
$$\mathbf{x}_{13}^d = [0.26\,\mathrm{m} \quad 0\,\mathrm{m/s} \quad 1.2\pi\mathrm{rad} \quad 0\mathrm{rad/s}]^T \tag{48}$$

The state variables and the control inputs are also similar to the formation task in Figure 4 as proven in Theorem 1 so that these curves are not be demonstrated, owing to the limited space.

Triangular formation moving along a U-shape trajectory. This platform in Figure 12 forms up a triangle when moving along a U-shape trajectory. Both the super-twisting sliding mode control parameters and the ELM parameters are kept unchanged. They are the same as the formation task in Figure 4. Concerning this task, the initial postures of the three robots are set by

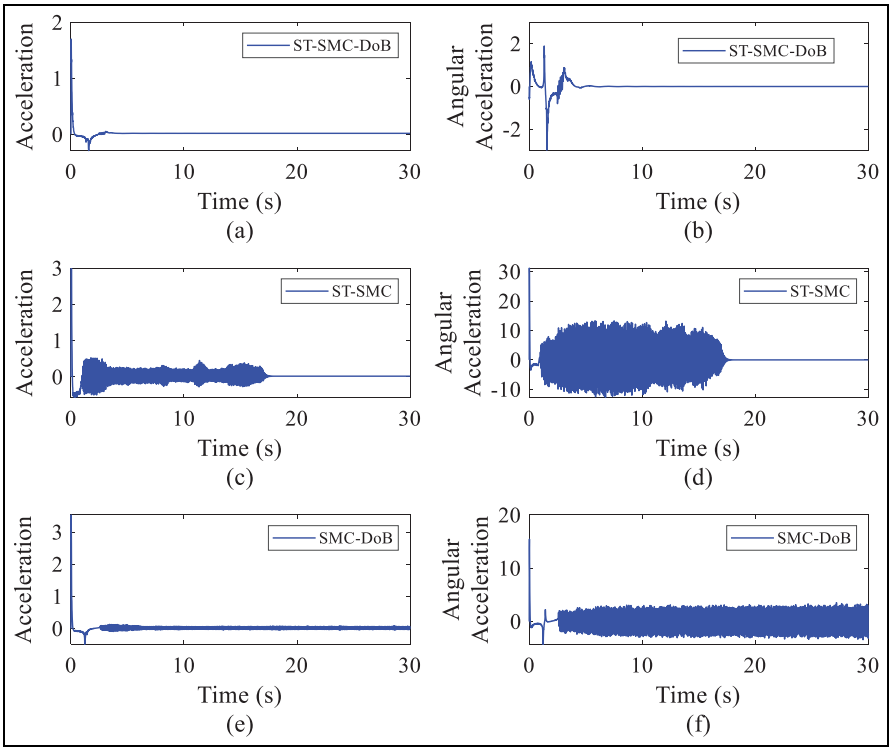

Figure 6. Comparisons of the control inputs from the follower 2: (a) acceleration by the ST-SMC-DoB, (b) angular acceleration by the ST-SMC-DoB, (c) acceleration by the ST-SMC, (d) angular acceleration by the ST-SMC, (e) acceleration by the SMC-DoB, and (f) angular acceleration by the SMC-DoB.

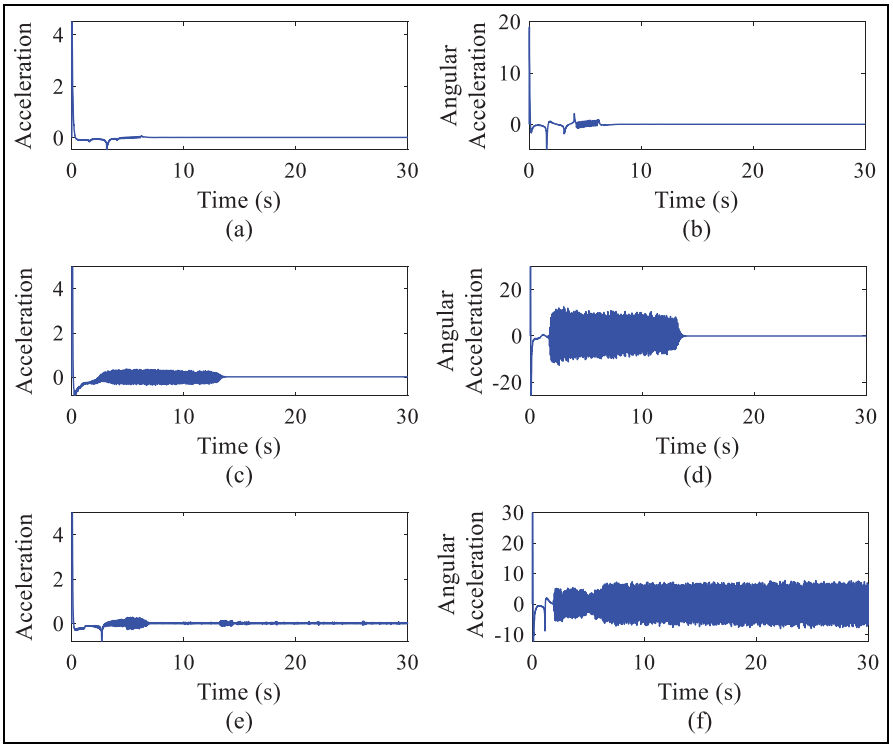

Figure 7. Comparisons of the control inputs from the follower 3: (a) acceleration by the ST-SMC-DoB, (b) angular acceleration by the ST-SMC-DoB, (c) acceleration by the ST-SMC, (d) angular acceleration by the ST-SMC, (e) acceleration by the SMC-DoB, and (f) angular acceleration by the SMC-DoB.

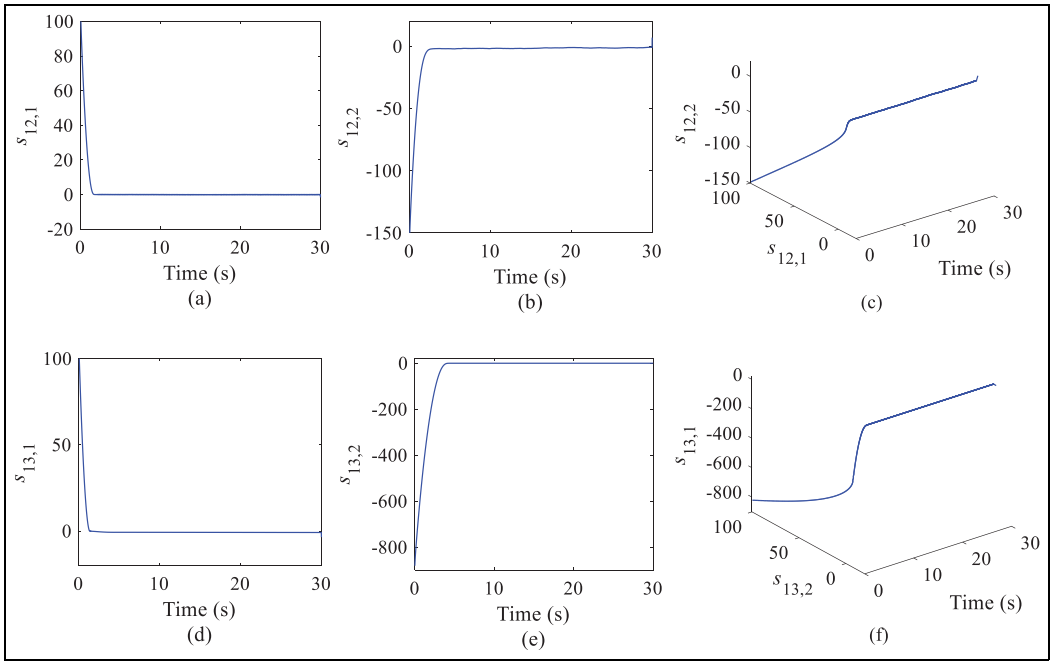

Figure 8. Sliding surfaces of the two followers: (a) $s_{12,1}$, (b) $s_{12,2}$, (c) $\mathbf{s}_{12}$, (d) $s_{13,1}$., (e) $s_{13,2}$, and (f) $\mathbf{s}_{13}$.

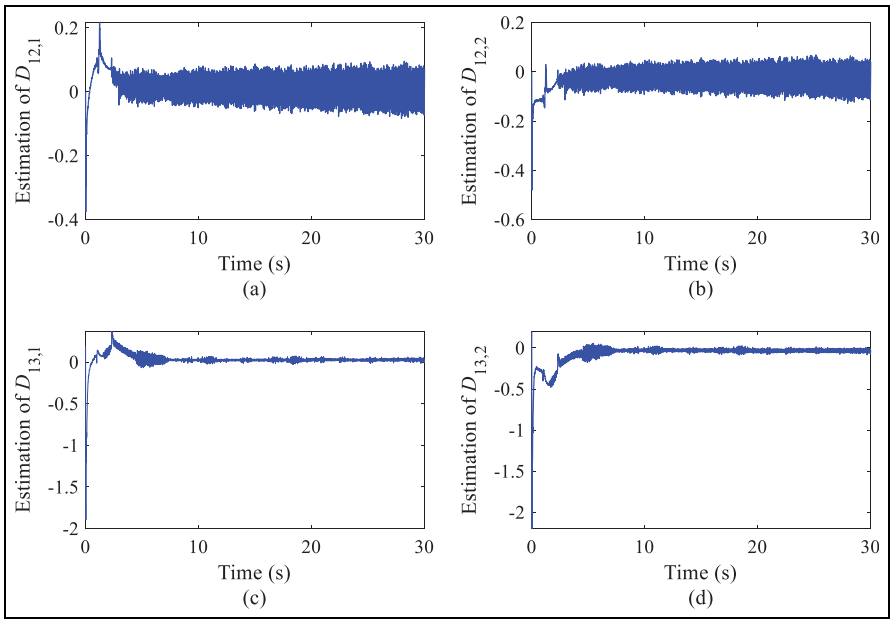

Figure 9. Disturbance observer outputs of the two followers: (a) estimation of $D_{12,1}$, (b) estimation of $D_{12,2}$, (c) estimation of $D_{13,1}$, and (d) estimation of $D_{13,2}$.

$$\mathbf{q}_1 = [0.5\,\mathrm{m} \quad 0\,\mathrm{m} \quad 0.5\pi\mathrm{rad}]^T,$$
$$\mathbf{q}_2 = [0.8\,\mathrm{m} \quad 0.1\,\mathrm{m} \quad 0.5\pi\mathrm{rad}]^T, \text{ and}$$
$$\mathbf{q}_3 = [1.2\,\mathrm{m} \quad 0.2\,\mathrm{m} \quad 0.33\pi\mathrm{rad}]^T \tag{49}$$

According to this control task and the initial postures, the initial states of the formation dynamics can be calculated by

$$\mathbf{x}_{12}(0) = [0.36\,\mathrm{m} \quad 0\,\mathrm{m/s} \quad 1.63\pi\mathrm{rad} \quad 0\ \mathrm{rad/s}]^T \text{ and}$$
$$\mathbf{x}_{12}(0) = [0.68\,\mathrm{m} \quad 0\,\mathrm{m/s} \quad 1.59\pi\mathrm{rad} \quad 0\ \mathrm{rad/s}]^T \tag{50}$$

Similarly, the desired states can be obtained on account of the leader's trajectory

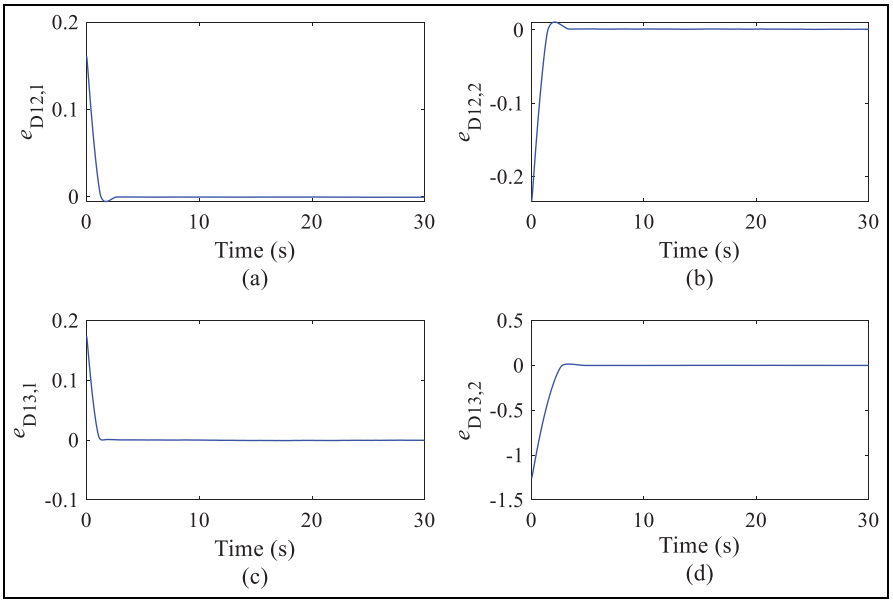

Figure 10. Estimation errors of the disturbance observers for the two followers: (a) $e_{D12,1}$, (b) $e_{D12,2}$, (c) $e_{D13,1}$, and (d) $e_{D13,2}$.

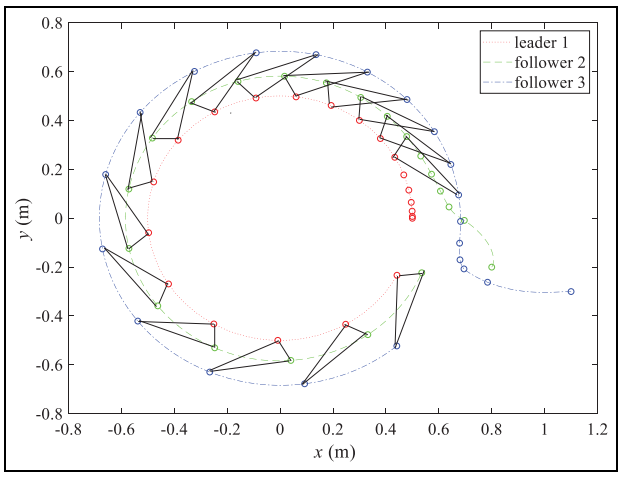

Figure 11. Triangular formation of this multi-robot platform when moving along a circular trajectory.

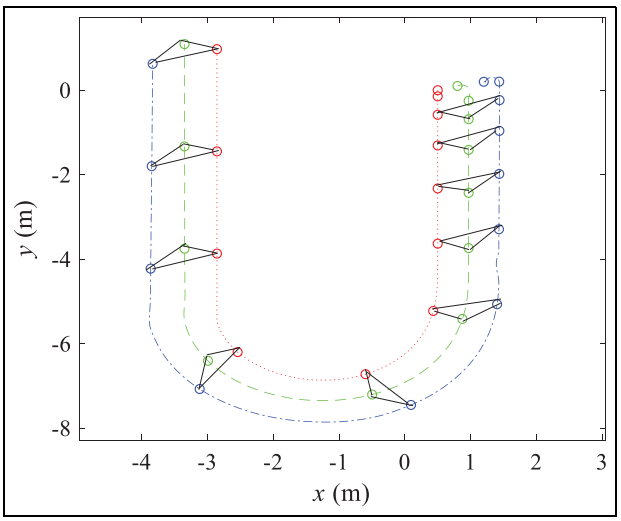

Figure 12. Triangular formation of this multi-robot platform when moving along a U-shape trajectory.

$$\mathbf{x}_{12}^{d} = [0.5\,\mathrm{m} \quad 0\,\mathrm{m/s} \quad 1.4\pi\mathrm{rad} \quad 0\ \mathrm{rad/s}]^{T} \text{ and}$$
$$\mathbf{x}_{13}^{d} = [1\,\mathrm{m} \quad 0\,\mathrm{m/s} \quad 1.6\pi\mathrm{rad} \quad 0\ \mathrm{rad/s}]^{T} \tag{51}$$

The state variables and the control inputs are also similar to the formation task in Figure 4 as proven in Theorem 1 so that these curves are not be demonstrated, owing to the limited space.

Conclusion

This paper has investigated the formation control problem of multi-agent mobile robots. In order to fulfill the formation task and resist the inevitable uncertainties and disturbances, the super-twisting sliding mode control method is adopted, which suffers from the overestimate of the control gains. Motivated by the improvement of the formation performance, the disturbance observer technique is deduced. Theoretically, the integration of the super-twisting sliding mode control and the disturbance observer for the formation maneuvers has the guaranteed stability in the sense of Lyapunov. In reality, the method is applied to a multi-robot platform with three mobile robots. Some comparisons via other two control methods have been illustrated, that is, the sliding mode control with disturbance observer and the sole super-twisting sliding mode control. Although all the three methods can realize the formation tasks, the numerical results demonstrate that the integrated method has the best performance. This method can be a solid support to deal with the formation maneuvers of multi-agent mobile robots.

Declaration of conflicting interests

The author(s) declared no potential conflicts of interest with respect to the research, authorship, and/or publication of this article.

Funding

The author(s) disclosed receipt of the following financial support for the research, authorship, and/or publication of this article: The work is supported by BJNSF(L191021) and National Science and Technology Major Project(2017-I-0006-0007).

ORCID iDs

Guigang Zhang https://orcid.org/0000-0002-1543-0770
Dianwei Qian https://orcid.org/0000-0001-7153-7997

References

1. Lin YL, Zhou HT, Chen MY, et al. Automatic sorting system for industrial robot with 3D visual perception and natural language interaction. *Meas Control* 2019; 52(1–2): 100–115.
2. Jiang C and Ueno S. Posture maintenance control of 2-link object by nonprehensile two-cooperative-arm robot without compensating friction. *IEEE/CAA J Autom Sinica* 2019; 6(6): 1397–1403.
3. Chen XL, Zhao H, Zhen SC, et al. Adaptive robust control for a lower limbs rehabilitation robot running under passive training mode. *IEEE/CAA J Autom Sinica* 2019; 6(2): 493–502.
4. Qian DW and Xi YF. Leader-follower formation maneuvers for multi-robot systems via derivative and integral terminal sliding mode. *Appl Sci* 2018; 8(7): 1045.
5. Onkol M and Kasnakoglu C. Adaptive model predictive control of a two-wheeled robot manipulator with varying mass. *Meas Control* 2018; 51(1–2): 38–56.
6. Yoo SJ and Park BS. Connectivity preservation and collision avoidance in networked nonholonomic multi-robot formation systems: unified error transformation strategy. *Automatica* 2019; 103: 274–281.
7. Qian DW, Tong SW and Li CD. Observer-based leader-following formation control of uncertain multiple agents by integral sliding mode. *Bull Pol Acad Sci Tech Sci* 2017; 65(1): 35–44.
8. Qian DW, Tong SW, Guo JR, et al. Leader-follower-based formation control of non-holonomic mobile robots with mismatched uncertainties via integral sliding mode. *Proc Inst Mech Eng Part I J Syst Control Eng* 2015; 229(6): 559–569.
9. Sun L. Saturated adaptive output-constrained control of cooperative spacecraft rendezvous and docking. *IEEE/CAA J Autom Sinica* 2019; 6(6): 1462–1470.
10. Park MJ, Kwon OM and Ryu JH. A Katz-centrality-based protocol design for leader-following formation of discrete-time multi-agent systems with communication delays. *J Frankl Inst Eng Appl Math* 2018; 355(13): 6111–6131.
11. Sun N, Wu Y, Chen H, et al. Antiswing cargo transportation of underactuated tower crane systems by a nonlinear controller embedded with an integral term. *IEEE Trans Autom Sci Eng* 2019; 16(3): 1387–1398.
12. Sun N, Liang D, Wu Y, et al. Adaptive control for pneumatic artificial muscle systems with parametric uncertainties and unidirectional input constraints. *IEEE Trans Ind Inform* 2020; 16(2): 969–979.
13. Bian T and Jiang ZP. Reinforcement learning for linear continuous-time systems: an incremental learning approach. *IEEE/CAA J Autom Sinica* 2019; 6(2): 433–440.
14. Jin X. Nonrepetitive leader-follower formation tracking for multiagent systems with LOS range and angle constraints using iterative learning control. *IEEE Trans Cybern* 2019; 49(5): 1748–1758.
15. Nascimento TP, Conceicao AGS and Moreira AP. Multi-robot nonlinear model predictive formation control: the obstacle avoidance problem. *Robotica* 2016; 34(3): 549–567.
16. Li CD, Yi JQ, Wang HK, et al. Interval data driven construction of shadowed sets with application to linguistic word modeling. *Inf Sci* 2020; 507: 503–521.
17. Peng W, Li CD, Zhang G, et al. Interval type-2 fuzzy logic based transmission power allocation strategy for lifetime maximization of WSNs. *Eng Appl Artif Intell* 2020; 87: 103269.
18. Qian DW, Tong SW and Li CD. Leader-following formation control of multiple robots with uncertainties through sliding mode and nonlinear disturbance observer. *ETRI J* 2016; 38: 1008–1018.
19. Qian DW, Li CD, Lee SG, et al. Robust formation maneuvers through sliding mode for multi-agent systems with uncertainties. *IEEE/CAA J Autom Sinica* 2018; 5(1): 342–351.
20. Nair RR, Karki H, Shukla A, et al. Fault-tolerant formation control of nonholonomic robots using fast adaptive gain nonsingular terminal sliding mode control. *IEEE Syst J* 2018; 13(1): 1006–1017.
21. Utkin VI. Discussion aspects of high-order sliding mode control. *IEEE Trans Autom Control* 2016; 61(3): 829–833.
22. Uppal AA, Alsmadi YM, Utkin VI, et al. Sliding mode control of underground coal gasification energy conversion process. *IEEE Trans Control Syst Technol* 2018; 26(2): 587–598.
23. Utkin VI and Poznyak AS. Adaptive sliding mode control with application to super-twist algorithm: equivalent control method. *Automatica* 2013; 49(1): 39–47.
24. Tian C, Li CD, Zhang G, et al. Data driven parallel prediction of building energy consumption using generative adversarial nets. *Energy Build* 2019; 186: 230–243.
25. Zhang M, Zhang Y, Chen H, et al. Model-independent PD-SMC method with payload swing suppression for 3D overhead crane systems. *Mech Syst Signal Proc* 2019; 129: 381–393.
26. Ouyang HM, Xu X and Zhang GM. Energy-shaping-based nonlinear controller design for rotary cranes with double-pendulum effect considering actuator saturation. *Autom Constr* 2020; 111: 103054.
27. Chen WH, Yang J, Guo L, et al. Disturbance-observer-based control and related methods: an overview. *IEEE Trans Ind Electron* 2016; 63(2): 1083–1095.
28. Mohammadi A, Marquez HJ and Tavakoli M. Nonlinear disturbance observers: design and applications to Euler-Lagrange systems. *IEEE Control Syst Mag* 2017; 37(4): 50–72.
29. Zhang M, Zhang Y and Cheng X. An enhanced coupling PD with sliding mode control method for underactuated double-pendulum overhead crane systems. *Int J Control Autom Syst* 2019; 17(6): 1579–1588.

30. Ouyang HM, Xu X and Zhang GM. Tracking and load sway reduction for double-pendulum rotary cranes using adaptive nonlinear control approach. *Int J Robust Nonlinear Control*. Epub ahead of print 13 December 2019. DOI: 10.1002/rnc.4854.
31. Qian DW, Tong SW and Lee SG. Fuzzy-logic-based control of payloads subjected to double-pendulum motion in overhead cranes. *Autom Constr* 2016; 65: 133–143.
32. Yang J, Li SH, Chen XS, et al. Disturbance rejection of dead-time processes using disturbance observer and model predictive control. *Chem Eng Res Des* 2011; 89(2): 125–135.
33. Qian DW, Ding H, Lee SG, et al. Suppression of chaotic behaviors in a complex biological system by disturbance observer-based derivative-integral terminal sliding mode. *IEEE/CAA J Autom Sinica* 2020; 7(1): 126–135.
34. Piao MN, Yang ZH, Sun MW, et al. A practical attitude control scheme for hypersonic vehicle based on disturbance observer. *Proc Inst Mech Eng Part G J Aerosp Eng* 2019; 233(12): 4523–4540.